Hyperglycemia induces microglial pyroptosis by increasing oxygen extraction rate: Implication in neurological impairment during ischemic stroke

ENSI LUO[1*], ZHUO LI[2*], SHIYING ZHANG[2*], YIN WEN[2], ZIXI YANG[3], HONGKE ZENG[2] and HONGGUANG DING[4]

[1]Department of Endocrinology, Binhaiwan Central Hospital of Dongguan, Dongguan Hospital Affiliated to Medical College of Jinan University, Dongguan, Guangdong 523903, P.R. China; [2]Department of Critical Care Medicine, Guangdong Provincial People's Hospital (Guangdong Academy of Medical Sciences), Southern Medical University, Guangzhou, Guangdong 510080, P.R. China; [3]College of Continuing Education, Guangdong Medical University, Zhanjiang, Guangdong 524023, P.R. China; [4]Department of Emergency Medicine, Guangdong Provincial People's Hospital (Guangdong Academy of Medical Sciences), Southern Medical University, Guangzhou, Guangdong 510080, P.R. China

Received January 17, 2024; Accepted May 31, 2024

DOI: 10.3892/mmr.2024.13270

Abstract. Elevated levels of blood glucose in patients with ischemic stroke are associated with a worse prognosis. The present study aimed to explore whether hyperglycemia promotes microglial pyroptosis by increasing the oxygen extraction rate in an acute ischemic stroke model. C57BL/6 mice that underwent middle cerebral artery occlusion were used for assessment of blood glucose level and neurological function. The cerebral oxygen extraction ratio ($CERO_2$), oxygen consumption rate (OCR) and partial pressure of brain tissue oxygen ($PbtO_2$) were measured. To investigate the significance of the NOD-like receptor protein 3 (NLRP3) inflammasome, $NLRP3^{-/-}$ mice were used, and the expression levels of NLRP3, caspase-1, full-length gasdermin D (GSDMD-FL), GSDMD-N domain (GSDMD-N), IL-1β and IL-18 were evaluated. In addition, Z-YVAD-FMK, a caspase-1 inhibitor, was used to treat microglia to determine whether activation of the NLRP3 inflammasome was required for the enhancing effect of hyperglycemia on pyroptosis. It was revealed that hyperglycemia accelerated cerebral injury in the acute ischemic stroke model, as evidenced by decreased latency to fall and the percentage of foot fault. Hyperglycemia aggravated hypoxia by increasing the oxygen extraction rate, as evidenced by increased $CERO_2$ and OCR, and decreased $PbtO_2$ in response to high glucose treatment. Furthermore, hyperglycemia-induced microglial pyroptosis was confirmed by detection of increased levels of caspase-1, GSDMD-N, IL-1β and IL-18 and a decreased level of GSDMD-FL. However, the knockout of NLRP3 attenuated these effects. Pharmacological inhibition of caspase-1 also reduced the expression levels of GSDMD-N, IL-1β and IL-18 in microglial cells. These results suggested that hyperglycemia stimulated NLRP3 inflammasome activation by increasing the oxygen extraction rate, thus leading to the aggravation of pyroptosis following ischemic stroke.

Correspondence to: Professor Hongke Zeng, Department of Critical Care Medicine, Guangdong Provincial People's Hospital (Guangdong Academy of Medical Sciences), Southern Medical University, 106 Zhongshan Er Road, Guangzhou, Guangdong 510080, P.R. China
E-mail: zenghongke@gdph.org.cn

Dr Hongguang Ding, Department of Emergency Medicine, Guangdong Provincial People's Hospital (Guangdong Academy of Medical Sciences), Southern Medical University, 106 Zhongshan Er Road, Guangzhou, Guangdong 510080, P.R. China
E-mail: dinghongguang@gdph.org.cn

*Contributed equally

Key words: ischemic stroke, hyperglycemia, pyroptosis, oxygen extraction, neuroinflammation

Introduction

Ischemic stroke is a common type of cerebrovascular disorder, and one of the leading global causes of death and serious disability (1). The 2022 American Heart Association report on Heart Disease and Stroke Statistics reported that the incidence rates of ischemic stroke were as high as 211/100,000 men and 174/100,000 women (2), resulting in a global annual economic burden (3). Early recognition and timely hospital treatments can significantly reduce stroke-related morbidity and mortality (3).

A number of researchers have reported that hyperglycemia during acute ischemic stroke is frequently observed as a result of chronic diabetes or an acute stress response (4). Acutely elevated levels of blood glucose in patients are associated with a worse prognosis and higher mortality (5). It has been reported that acute hyperglycemia can augment neuroinflammation, cause greater infarction area and increase the risk of hemorrhagic transformation (6,7). In light of these findings,

the mechanism underlying how hyperglycemia deteriorates acute ischemic stroke remains to be investigated.

Microglia act as the immune cells in the central nervous system and play an essential role in the pathogenesis of ischemic stroke (8). Recent research has found that intracellular NOD-like receptors, such as NOD-like receptor protein 3 (NLRP3), are widely expressed in microglia (9). The NLRP3 inflammasome, which consists of NLRP3, apoptosis-associated speck-like protein and pro-caspase-1, has been proven to be associated with the deterioration of the disease condition (10). Activation of the NLRP3 inflammasome upregulates the expression of caspase-1 to process full-length gasdermin D (GSDMD-FL) to GSDMD-N domain (GSDMD-N), thus causing the release of IL-1β and IL-18 (11). As a result of this inflammatory response, pyroptosis can occur (12). It has been reported that pyroptosis in vascular cells plays an important role in vascular inflammation-induced blood-brain barrier breakdown in diabetes-associated cognitive decline (13). Tissue plasminogen activator can promote NLRP3 inflammasome activation after hyperglycemic stroke in mice (14). However, whether the elevation of blood glucose deteriorates cerebral injury via microglial pyroptosis in acute ischemic stroke needs further exploration.

The present study aimed to explore whether hyperglycemia promotes microglial pyroptosis via increasing oxygen extraction rate in an acute ischemic stroke model.

Materials and methods

Animals. The NLRP3 knockout (KO) C57BL/6 mice ($NLRP3^{-/-}$; male; age, 6 weeks) were purchased from GemPharmatech Co., Ltd. The age-matched male wild-type (WT) littermates were used as controls. The mice were fed standard chow and water, and were housed under standard experimental conditions (temperature, 20-25˚C; humidity, 50-70%) under a 12-h light/dark cycle. The weight range of the mice was 18.22-21.56 g, with a median of 19.34 g. The mice were randomly divided into the following groups: i) Sham-operated group (Sham); ii) ischemia-reperfusion (IR) group; iii) IR + normal glucose group (IR + NG); iv) IR + high glucose group (IR + HG); v) $NLRP3^{-/-}$ + IR + HG group; and vi) IR + HG + Z-YVAD-FMK (a caspase-1 inhibitor) group. The mice in the $NLRP3^{-/-}$ + IR + HG group underwent IR and were treated once with a high level of glucose at a rate of 2.5 g/(kg x h) for 2 h (total dose, 5 g/kg). Mice in the IR + HG + Z-YVAD-FMK group were intraperitoneally injected with Z-YVAD-FMK at a dose of 12.5 mg/kg prior to IR. The number of mice in each group was 36. The mice were allowed free access to standard chow and water, and were housed under standard experimental conditions in a specific pathogen-free environment (temperature, 20-25˚C; humidity, 50-70%) with a 12-h light/dark cycle.

The entire experimental course consisted of 2 h of ischemia and 24 h of reperfusion. Animals were anesthetized with sodium pentobarbital (30 mg/kg; i.p.) before surgery. The health and behavior of the mice were examined every half hour. If the mice showed signs of awakening during the experiment, sodium pentobarbital (10 mg/kg; i.p.) was supplemented. A total of 22 mice died during the experiment and the rest were euthanized. Respiratory and circulatory failure caused by cerebral edema after cerebral infarction were considered the main cause of death. It has been reported that the mortality rate of mice with middle cerebral artery occlusion (MCAO) was 15% (15), which is consistent with the results (11.96%, 22/184) in the present study.

Euthanasia was performed if mice had difficulty breathing, or became emaciated or dehydrated due to not eating or drinking for 24-48 h. Mice were euthanized by injection with pentobarbital (30 mg/kg; i.p.), followed by cervical dislocation. Heartbeat and breathing were checked to ensure successful euthanasia. All animal experimental procedures including accidental death and euthanasia were approved by The Research Ethics Committee of Guangdong Provincial People's Hospital (Guangzhou, China; approval no. GDRECKY2020-046-01) and were performed following the ARRIVE 2.0 guidelines (16).

MCAO and glucose treatment. Animals were anesthetized with sodium pentobarbital (30 mg/kg intraperitoneal injection) before surgery. As previously described, MCAO was used to establish transient focal cerebral ischemia (15). Briefly, the right middle cerebral artery was blocked with a nylon suture, which was inserted into the internal carotid artery and advanced until the origin of the right middle cerebral artery was closed. After a 2-h occlusion, the suture was removed for reperfusion. The sham mice were subjected to a similar operation, except for the occlusion. During the period of MCAO, high glucose (50% glucose) or normal glucose (5% glucose) was injected through the caudal vein at a rate of 5 ml/(kg x h). The blood glucose levels before, and 2 and 24 h after ischemia were measured using the StatStrip Xpress Glucose Meter (Nova Biomedical Corporation). In addition, 2,3,5,-triphenyl tetrazolium chloride monohydrate (TTC) assessment was used to verify the establishment of the MCAO model. Briefly, brains were removed and cut into 2-mm-thick slices after sacrifice. The slices were immersed in 1% TTC for 30 min at 37˚C and fixed with 10% formalin for 6 h at 4˚C. Infarcted brain tissue was pale, while normal brain tissue was red. All mice in the IR group developed cerebral infarction (100%), while no mice in the Sham group developed cerebral infarction (0%).

Measurement of partial pressure of brain tissue oxygen ($PbtO_2$). The levels of $PbtO_2$ were measured according to a previously reported procedure (17). Briefly, a midline incision was performed, a hole was drilled and the dura was punctured. A microsensor was then inserted into the brain tissue. The $PbtO_2$ was measured at 1, 3, 6, 12 and 24 h after reperfusion using a monitor (Integra CAMO2; Integra LifeSciences Corporation).

Measurement of cerebral oxygen extraction ratio ($CERO_2$). The levels of $CERO_2$ were measured as described previously (17). The right jugular vein was cannulated upstream to collect venous blood from the right side of the brain at 1, 3, 6, 12 and 24 h after reperfusion. Arterial blood samples were also collected from the femoral artery. The blood gas analysis was performed using a blood gas/electrolyte analyzer (Model 5700; Werfen, S.A.). Tests included hemoglobin concentration (Hb), saturation of arterial blood oxygen (SaO_2), saturation of jugular venous blood oxygen, partial pressure of oxygen (PaO_2) and pressure of jugular venous blood oxygen ($PjVO_2$).

The content of jugular venous blood oxygen ($CjVO_2$), content of arterial blood oxygen (CaO_2) and $CERO_2$ were calculated using the following formulas:

$$CaO_2=1.36 \times Hb \times SaO_2 + 0.0031 \times PaO_2$$

$$CjVO_2=1.36 \times Hb \times PjVO_2 + 0.0031 \times PjVO_2$$

$$CERO_2=(CaO_2-CjVO_2)/CaO_2$$

Neurological tests. The neurological damage to the motor center of the cerebral cortex after IR was examined by rotarod and foot fault tests. The rotarod test was used to assess the coordination and body strength of the mice. The mice were placed on a six-lane acceleration rotary paddle at a rotation rate of 120 rpm and the residence time was recorded. The foot fault test was performed to evaluate limb motor function. Mice were placed on a metal mesh (area, 3 cm^2) for 2 min and the number of missing steps on the left foreleg was subsequently recorded. Percentage of foot fault (%)=the number of missing steps/total steps.

Primary microglia isolation and culture. Primary microglia were obtained from the brain cortexes of newborn WT or $NLRP3^{-/-}$ mice (male; age, 1-3 days; weight, 2-3 g), as previously described (17). A total of 40 newborn mice were purchased from GemPharmatech Co., Ltd., and were sacrificed immediately after purchase. Briefly, the mice were anesthetized with sodium pentobarbital (30 mg/kg intraperitoneal injection) and sacrificed by cervical dislocation. Heartbeat and breathing were checked to ensure successful euthanasia. The cortexes were isolated from the entire brain under sterile conditions and the meninges were removed under a dissecting microscope. After which, the cortexes were cut into pieces as large as 1x1 mm and were digested with trypsin for 10 min. The cell suspension was placed in a 15-ml poly-L-lysine-coated flask and cultured in Dulbecco's modified Eagle's medium (DMEM) supplemented with 10% fetal bovine serum (FBS) at 37˚C and 5% CO_2 for 2 weeks. Afterwards, the mixed glial cells were shaken at 1.33 x g at 37˚C for 2 h to obtain microglia. The collected cells were seeded in 2-ml poly-L-lysine-coated plates and cultured in DMEM/F12 supplemented with 10% FBS at 37˚C. Primary microglia from WT mice were randomly divided into groups: i) Control group (CON); ii) oxygen and glucose deprivation (OGD) group; iii) OGD + NG group (OGD + NG); iv) OGD + HG group (OGD + HG); and v) OGD + HG + Z-YVAD-FMK (an inhibitor of caspase-1) group (OGD + HG + Z-YVAD-FMK). The microglia from the $NLRP3^{-/-}$ + OGD + HG group originated from $NLRP3^{-/-}$ mice, and were exposed to OGD and high glucose.

OGD treatment. Microglia in the OGD group were cultured in glucose-free DMEM and transferred to a hypoxic chamber with 95% N_2/5% CO_2/0.1% O_2 at 37˚C for 6 h. After 6 h of OGD, the cells were returned to high-glucose DMEM with 10% FBS at 37˚C in an incubator with 5% CO_2/95% air for 24 h, which was used to reflect IR injury of the ischemic penumbra in cortical areas *in vivo*. Cells in the OGD + HG group were treated with 25 mM glucose at 37˚C for 24 h following 6-h OGD. Meanwhile, the cells in the OGD + HG + Z-YVAD-FMK group were also treated with 10 μM Z-YVAD-FMK at 37˚C for 24 h.

Oxygen consumption rate (OCR) evaluation of microglial cells. The OCR was evaluated using a cellulate OCR Assay Kit (cat. no. BB-48211; Bebo Biotechnology), as previously described (17). Briefly, microglial cells were seeded in 96-well plates. After 6 h of OGD, the cells were restored to the supply of glucose and oxygen at 37˚C for 24 h. After which, oxygen fluorescent probes (BBoxiProbe® R01) and oxygen-mounting media were added to 96-well plates sequentially. The OCR levels were measured every 3 min using a fluorescence microplate reader (Model 9260; LI-COR Biosciences).

Western blotting. The brain tissue from the ischemic penumbra in the cortical area 24 h after ischemia, and primary microglial cells, were lysed on ice with RIPA lysis buffer (cat. no. BB-3101-100T; Bebo Biotechnology) containing protease inhibitors. Notably, there was a region of encephalomalacia following MCAO. The area around the encephalomalacia region was considered the ischemic penumbra. The brain tissue close to the surface of the cerebral hemisphere was extracted from the ischemic penumbra. The BCA protein assay kit (cat. no. 23227; Pierce; Thermo Fisher Scientific, Inc.) was used to measure the total protein concentration. After mixing with 4X loading buffer, the proteins (40 μg per lane) were separated by 10% SDS-PAGE and transferred onto PVDF membranes. Then, the membranes were blocked with 5% BSA (cat. no. V900933; Sigma-Aldrich; Merck KGaA) for 1 h at room temperature, and were incubated overnight at 4˚C with primary antibodies against caspase-1 (1:1,000; cat. no. ab138483; Abcam), GSDMD-FL (1:1,000; cat. no. ab219800; Abcam), GSDMD-N (1:1,000; cat. no. 10137; Cell Signaling Technology), IL-1β (1:1,000; cat. no. ab254360; Abcam), IL-18 (1:1,000; cat. no. ab191860; Abcam) and β-actin (1:1,000; cat. no. ab8226; Abcam). On the following day, the membranes were incubated with horseradish peroxidase-conjugated secondary antibodies (1:1,000; cat. no. 7074S; Cell Signaling Technology, Inc.) for 2 h at 4˚C. Finally, the blots were detected by enhanced chemiluminescence (MilliporeSigma) using an imaging densitometer (ImageQuant LAS 500; GE Healthcare Bio-Sciences).

Immunofluorescence. A total of 24 h after reperfusion, normal saline and 4% paraformaldehyde were injected transcardially under anesthesia, and the brain was immediately collected. The collected brain tissue was fixed with 4% paraformaldehyde for 24 h at 4˚C, dehydrated with gradient sucrose, and cut into 4-μm slices. The sections were permeabilized with 0.5% Triton X-100 for 30 min at room temperature and then blocked with and 1% BSA (cat. no. V900933; Sigma-Aldrich; Merck KGaA) for 30 min at room temperature. Thereafter, the following appropriate primary antibodies were applied at 4˚C overnight: Iba1 (1:200; cat. no. ab283346; Abcam), caspase-1 (1:200; cat. no. 24232; Cell Signaling Technology), GSDMD-N (1:200; cat. no. DF13758; Affinity), IL-1β (1:200; cat. no. ab254360; Abcam) and IL-18 (1:200; cat. no. ab191860; Abcam), followed by secondary antibody incubation for 1 h at room temperature, including Alexa Fluor® 488-conjugated goat anti-mouse IgG (1:200; cat. no. ab150113; Abcam) and Alexa Fluor® 594-conjugated donkey anti-rabbit IgG (1:200;

cat. no. ab150080; Abcam). Finally, the slices were sealed with mounting medium (cat. no. F6057; MilliporeSigma). The number of cells was decreased in the area of necrosis under a fluorescence microscope (Olympus DP73 Microscope; Olympus). The peripheries of this area were considered the ischemic penumbra. The ischemic penumbra close to the surface of the cerebral hemisphere was observed and imaged. The cells on coverslips were fixed with 4% paraformaldehyde, and the cells underwent permeabilization, blocking and antibody incubation as aforementioned. The average fluorescence (red) density of one single microglia was analyzed using an image analysis system (Image-Pro Plus software; version 7.0; Media Cybernetics, Inc.).

Statistical analyses. Statistical analysis was performed using SPSS version 22.0 (IBM Corp.). All data are expressed as the mean ± standard deviation. The experiments were repeated six times *in vivo* and four times *in vitro*. The Shapiro-Wilk test was performed to determine data distribution, and all data conformed to a normal distribution. An unpaired Student's t-test was used to analyze two-group measurement data. A one-way analysis of variance (ANOVA) was used to analyze the data of four, five or six-group univariate-factor measurements. Multiple comparisons were analyzed by Tukey's test following ANOVA. $P<0.05$ was considered to indicate a statistically significant difference.

Results

High glucose treatment aggravates neurological damage after IR. To investigate the effect of blood glucose levels on neurological function after IR, the blood glucose levels, latency time to fall and percentage of foot fault were assessed. The results demonstrated that there was no difference in blood glucose levels among the Sham, IR, IR + NG, IR + HG and IR + HG + NLRP3$^{-/-}$ groups at 0 h after ischemia ($P>0.05$; Fig. 1A). However, the blood glucose levels in the IR + HG and IR + HG + NLRP3$^{-/-}$ groups were significantly increased compared with the Sham, IR and IR + NG groups ($P<0.01$), and there was no difference among the Sham, IR and IR + NG groups, as well as between the IR + HG and IR + HG + NLRP3$^{-/-}$ groups at 2 and 24 h after ischemia ($P>0.05$; Fig. 1B and C). TTC staining images showed the cerebral infarction in the IR group. The incidence of cerebral infarction was 100% in the IR group, while that of the Sham group was 0% ($P<0.01$; Fig. 1D); this suggested that the establishment of the MCAO model was successful. The latency to fall in the IR and IR + NG groups were decreased compared with in the Sham group ($P<0.01$), and it was further decreased in response to high glucose ($P<0.01$). However, the latency to fall was significantly prolonged in the IR + HG + NLRP3$^{-/-}$ group compared with the IR + HG group ($P<0.01$; Fig. 1E). The percentage of foot fault in the IR groups was notably increased compared with in the Sham group ($P<0.01$) and it was further increased in response to high glucose ($P<0.05$). However, the percentage was significantly reduced in the IR + HG + NLRP3$^{-/-}$ group compared with the IR + HG group ($P<0.01$; Fig. 1F). These results suggested that high glucose can exert an aggravating effect on neurological damage after IR via activating the NLRP3 inflammasome.

High glucose treatment aggravates hypoxia via increasing oxygen extraction rate. The level of $CERO_2$ in the IR group was notably increased compared with that in the Sham group (1, 3, 6, 12 and 24 h; $P<0.01$) and it was further increased in response to high glucose (1, 3, 6 and 24 h: $P<0.01$; 12 h: $P<0.05$; Fig. 2A). The level of $PbtO_2$ in the IR group was significantly decreased compared with that in the Sham group (1, 3, 6, 12 and 24 h; $P<0.01$), and the IR + HG group had the lowest $PbtO_2$ level as compared with the IR group and Sham group (1 and 24 h, $P<0.05$; 3, 6 and 12 h, $P<0.01$; Fig. 2B). The level of OCR in the OGD group was notably increased compared with that in the CON group (5, 15 and 25 min, $P<0.05$; 10, 20 and 30 min, $P<0.01$) and it was further increased in response to high glucose (5, 15, 20 and 25 min, $P<0.01$; 10 and 30 min, $P<0.05$; Fig. 2C). These results suggested that high glucose treatment aggravated hypoxia by increasing the oxygen extraction rate.

NLRP3 KO inhibits microglial pyroptosis activation after IR. The level of NLRP3 in the KO group was notably decreased compared with that in the WT group ($P<0.01$), indicating that the NLRP3 KO model was successfully established (Fig. 3A and B). There was an increase in the expression of caspase-1 in the WT + IR group compared with in the WT + Sham group ($P<0.01$). By contrast, the expression of caspase-1 in the NLRP3$^{-/-}$ + IR group was notably decreased compared with in the WT + IR group ($P<0.01$; Fig. 3A and C). There was a decrease in the expression of GSDMD-FL in the WT + IR group compared with in the WT + Sham group ($P<0.01$). The expression of GSDMD-FL in the NLRP3$^{-/-}$ + IR group was notably increased compared with in the WT + IR group ($P<0.05$; Fig. 3A and D). There was an increase in the expression of GSDMD-N in the WT + IR group compared with in the WT + Sham group ($P<0.01$). The expression of GSDMD-N in the NLRP3$^{-/-}$ + IR group was notably decreased compared with in the WT + IR group ($P<0.01$; Fig. 3A and E). There was an increase in the expression of IL-1β in the WT + IR group compared with in the WT + Sham group ($P<0.01$). The expression of IL-1β in the NLRP3$^{-/-}$ + IR group was notably decreased compared with in the WT + IR group ($P<0.01$; Fig. 3A and F). There was an increase in the expression of IL-18 in the WT + IR group compared with in the WT + Sham group ($P<0.01$). By contrast, the expression of IL-18 in the NLRP3$^{-/-}$ + IR group was notably decreased compared with in the WT + IR group ($P<0.01$; Fig. 3A and G). These results suggested that IR can activate the NLRP3 inflammasome, and NLRP3 KO may inhibit activation of the NLRP3 inflammasome and the occurrence of pyroptosis.

NLRP3 KO inhibits high glucose-induced exacerbation of pyroptosis after IR. The expression levels of caspase-1, GSDMD-FL, GSDMD-N, IL-1β and IL-18 after high glucose treatment were analyzed. The results of western blotting revealed an increase in the expression of caspase-1 in the IR and IR + NG groups compared with in the Sham group ($P<0.05$); it was further increased in response to high glucose, whereas a decrease in the expression of caspase-1 was detected in the IR + HG + NLRP3$^{-/-}$ group compared with in the IR + HG group ($P<0.01$; Fig. 4A and B). The expression of GSDMD-FL in the IR and IR + NG groups was notably decreased compared with in the Sham group ($P<0.05$), which was further decreased

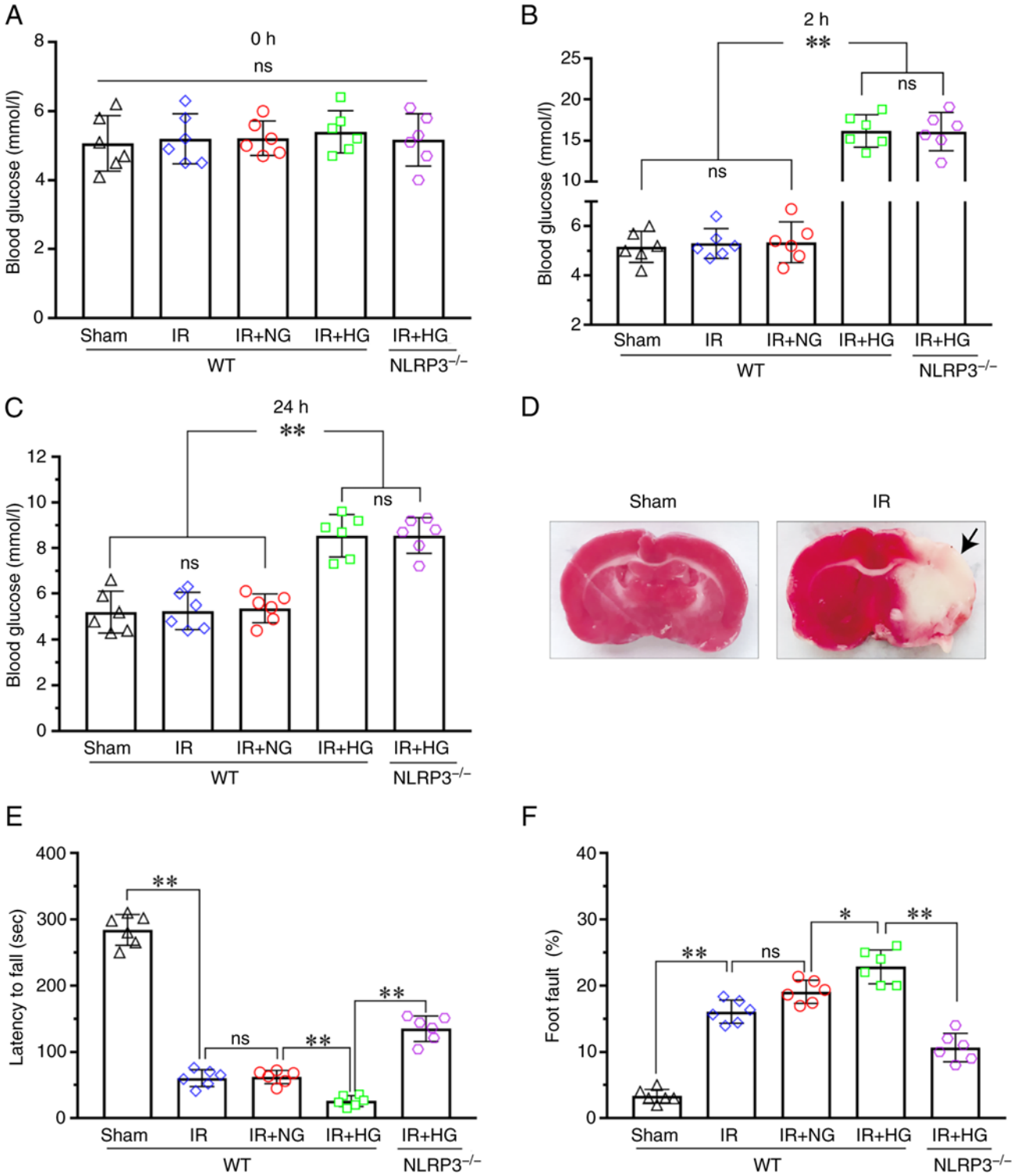

Figure 1. HG treatment aggravated neurological damage after IR. (A) Blood glucose levels of the mice at 0 h after ischemia. (B) Blood glucose levels of the mice at 2 h after ischemia. (C) Blood glucose levels of the mice at 24 h after ischemia. (D) TTC staining images showed cerebral infarction (black arrow) in the IR group. The incidence of cerebral infarction was 100% in the IR group, while in the Sham group it was 0% (P<0.01). (E) Latency to fall of the Sham, IR, IR + HG, IR + NG and IR + HG + NLRP3-/- groups. (F) Foot fault of the Sham, IR, IR + HG, IR + NG and IR + HG + NLRP3-/- groups. Data are presented as the mean ± standard deviation. *P<0.05; **P<0.01; ns, not significant. n=6 mice per group. IR, ischemia-reperfusion; NG, normal glucose; HG, high glucose; NLRP3, NOD-like receptor protein 3.

in response to high glucose (P<0.01), but was increased in the IR + HG + NLRP3$^{-/-}$ group compared with the IR + HG group (P<0.01; Fig. 4A and C). The results revealed an increase in the expression of GSDMD-N in the IR and IR + NG groups compared with in the Sham group (P<0.05), which was further increased in response to high glucose (P<0.01), but decreased in the IR + HG + NLRP3$^{-/-}$ group compared with the IR + HG group (P<0.01; Fig. 4A and D). Furthermore, the results revealed an increase in the expression of IL-1β in the IR and IR + NG groups compared with in the Sham group (P<0.05);

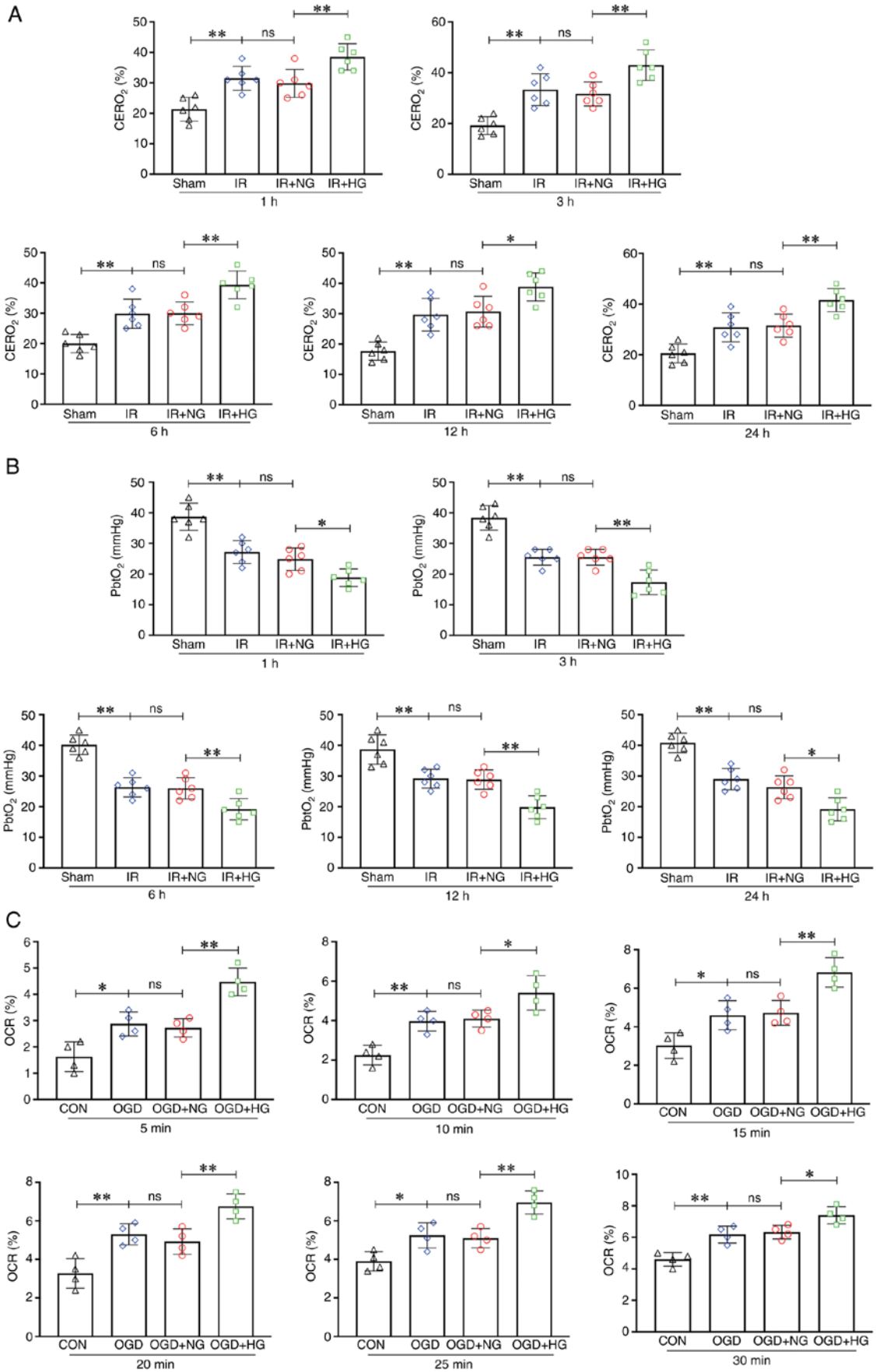

Figure 2. HG treatment aggravated hypoxia by increasing the oxygen extraction rate. (A) Levels of $CERO_2$ in the Sham, IR, IR + HG and IR + NG groups. (B) Levels of $PbtO_2$ in the Sham, IR, IR + HG and IR + NG groups. (C) Levels of OCR in the CON, OGD, OGD + HG and OGD + NG groups. Data are presented as the mean ± standard deviation. *P<0.05; **P<0.01; ns, not significant. n=4 per group *in vitro*, n=6 per group *in vivo*. IR, ischemia-reperfusion; OGD, oxygen and glucose deprivation; NG, normal glucose; HG, high glucose; $CERO_2$, cerebral oxygen extraction ratio; $PbtO_2$, partial pressure of brain tissue oxygen; OCR, oxygen consumption rate; CON, control.

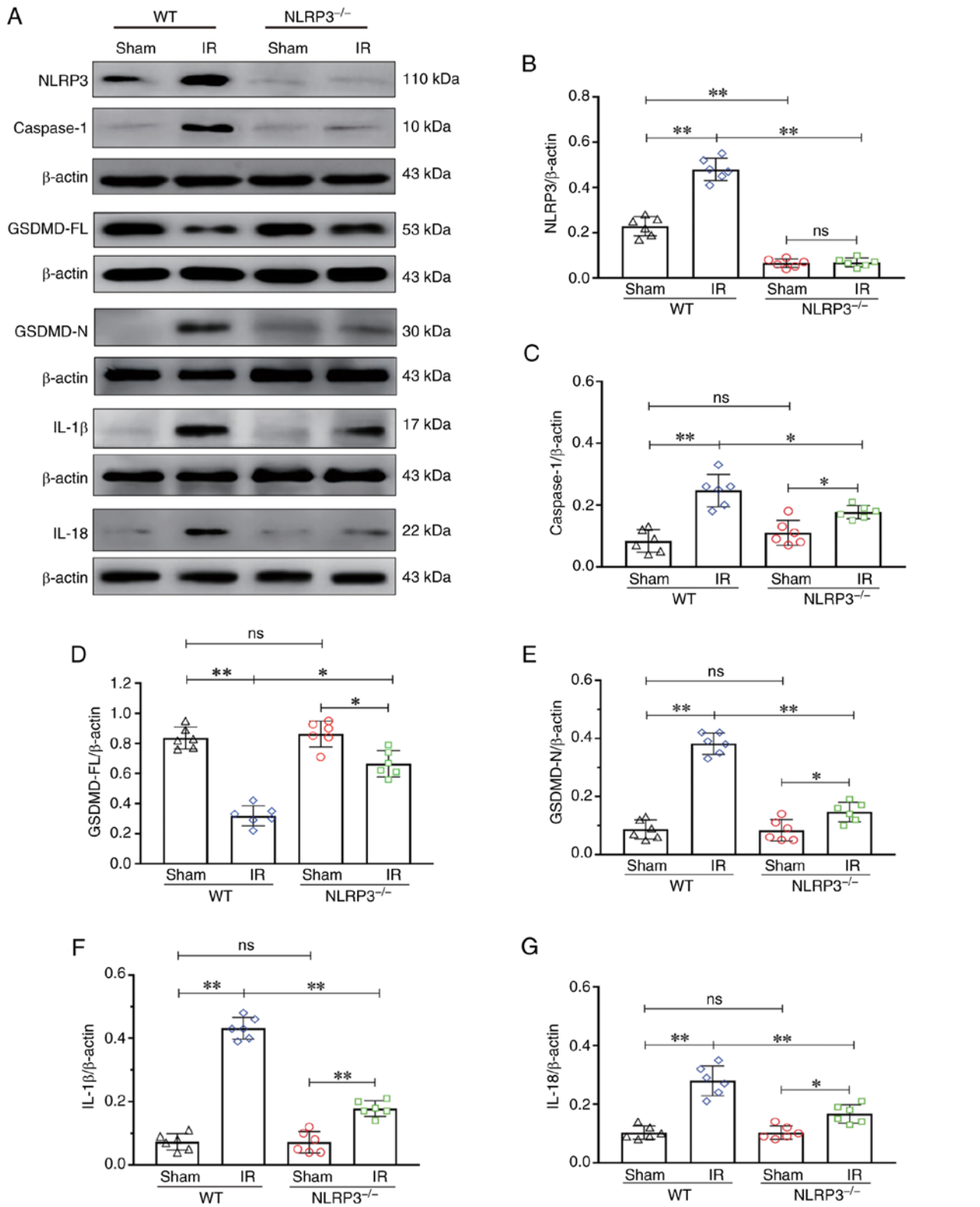

Figure 3. NLRP3$^{-/-}$ inhibited microglial pyroptosis activation after IR. (A) Western blot analysis of NLRP3 (110 kDa), caspase-1 (10 kDa), GSDMD-FL (53 kDa), GSDMD-N (30 kDa), IL-1β (17 kDa) and IL-18 (22 kDa). (B) NLRP3 expression. (C) Caspase-1 expression. (D) GSDMD-FL expression. (E) GSDMD-N expression. (F) IL-1β expression. (G) IL-18 expression. Data are presented as the mean ± standard deviation. *P<0.05; **P<0.01; ns, not significant. n=6 mice per group. IR, ischemia-reperfusion; NLRP3, NOD-like receptor protein 3; GSDMD-FL, full-length gasdermin D; GSDMD-N, gasdermin D-N domain; NLRP3$^{-/-}$; NLRP3 knockout; WT, wild-type.

it was further increased in response to high glucose (P<0.01), but a decrease in the expression of IL-1β was detected in the IR + HG + NLRP3$^{-/-}$ group compared with in the IR + HG group (P<0.01; Fig. 4A and E). The results revealed an increase in the expression of IL-18 in the IR and IR + NG groups compared with in the Sham group (P<0.05), which was further increased in response to high glucose (P<0.01), and a decrease in the expression of IL-18 was observed in the IR +

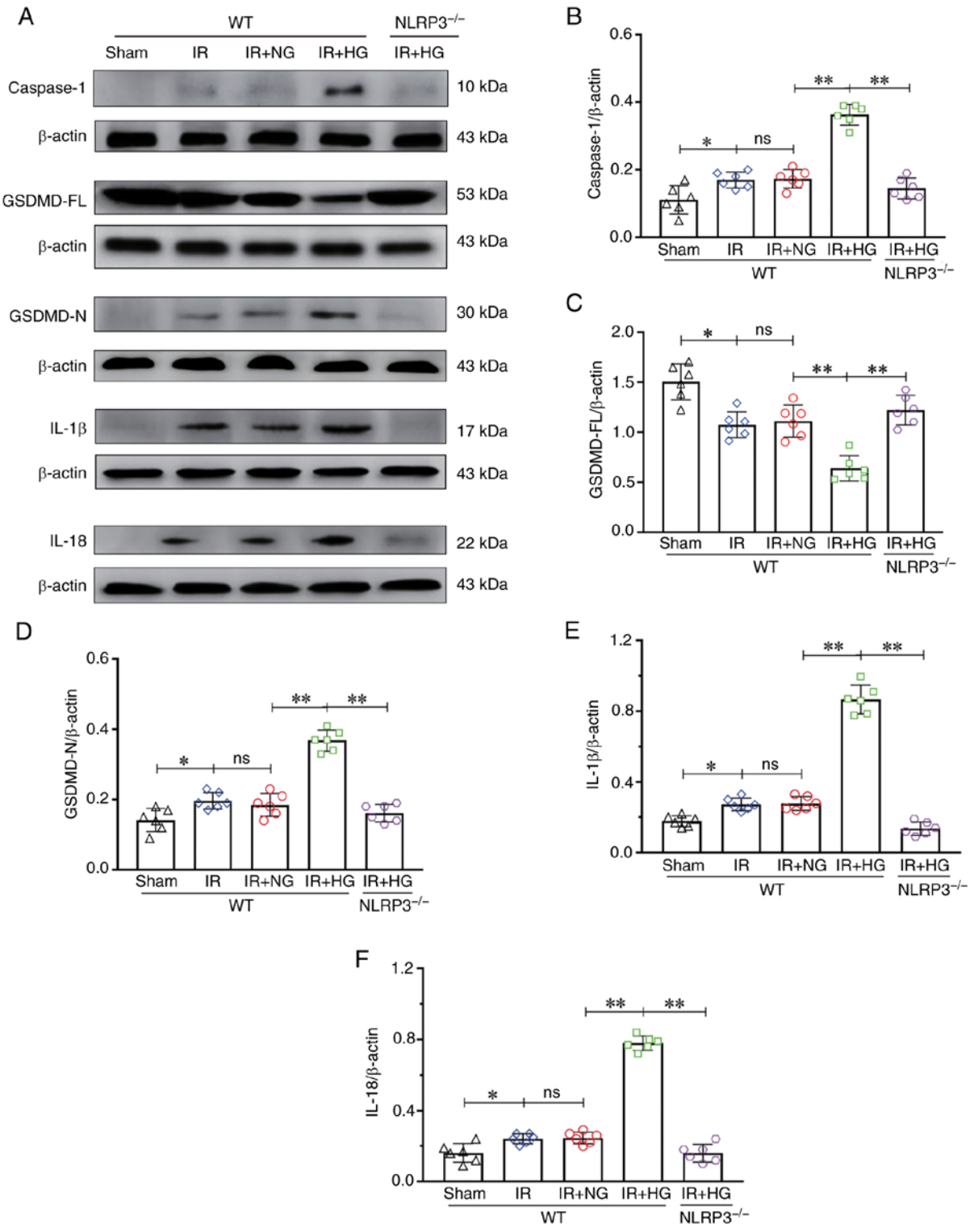

Figure 4. NLRP3$^{-/-}$ inhibited HG-induced exacerbation of pyroptosis after IR *in vivo*. (A) Western blot analysis of Caspase-1 (10 kDa), GSDMD-FL (53 kDa), GSDMD-N (30 kDa), IL-1β (17 kDa) and IL-18 (22 kDa). (B) Caspase-1 expression. (C) GSDMD-FL expression. (D) GSDMD-N expression. (E) IL-1β expression. (F) IL-18 expression. Data are presented as the mean ± standard deviation. *P<0.05; **P<0.01; ns, not significant. n=6 mice per group. IR, ischemia-reperfusion; NG, normal glucose; HG, high glucose; NLRP3, NOD-like receptor protein 3; GSDMD-FL, full-length gasdermin D; GSDMD-N, gasdermin D-N domain; NLRP3$^{-/-}$; NLRP3 knockout; WT, wild-type.

HG + NLRP3$^{-/-}$ group compared with in the IR + HG group (P<0.01; Fig. 4A and F).

To verify the effect of high glucose on microglial pyroptosis after IR *in vivo*, the expression levels of caspase-1, GSDMD-N, IL-1β and IL-18 in microglia was detected by double immunofluorescence. It was revealed that IR enhanced the expression of caspase-1 in cerebral microglial cells compared with in the Sham group, and this increase was substantially enhanced in the IR group treated with high glucose; however, the expression of caspase-1 was notably reduced after NLRP3

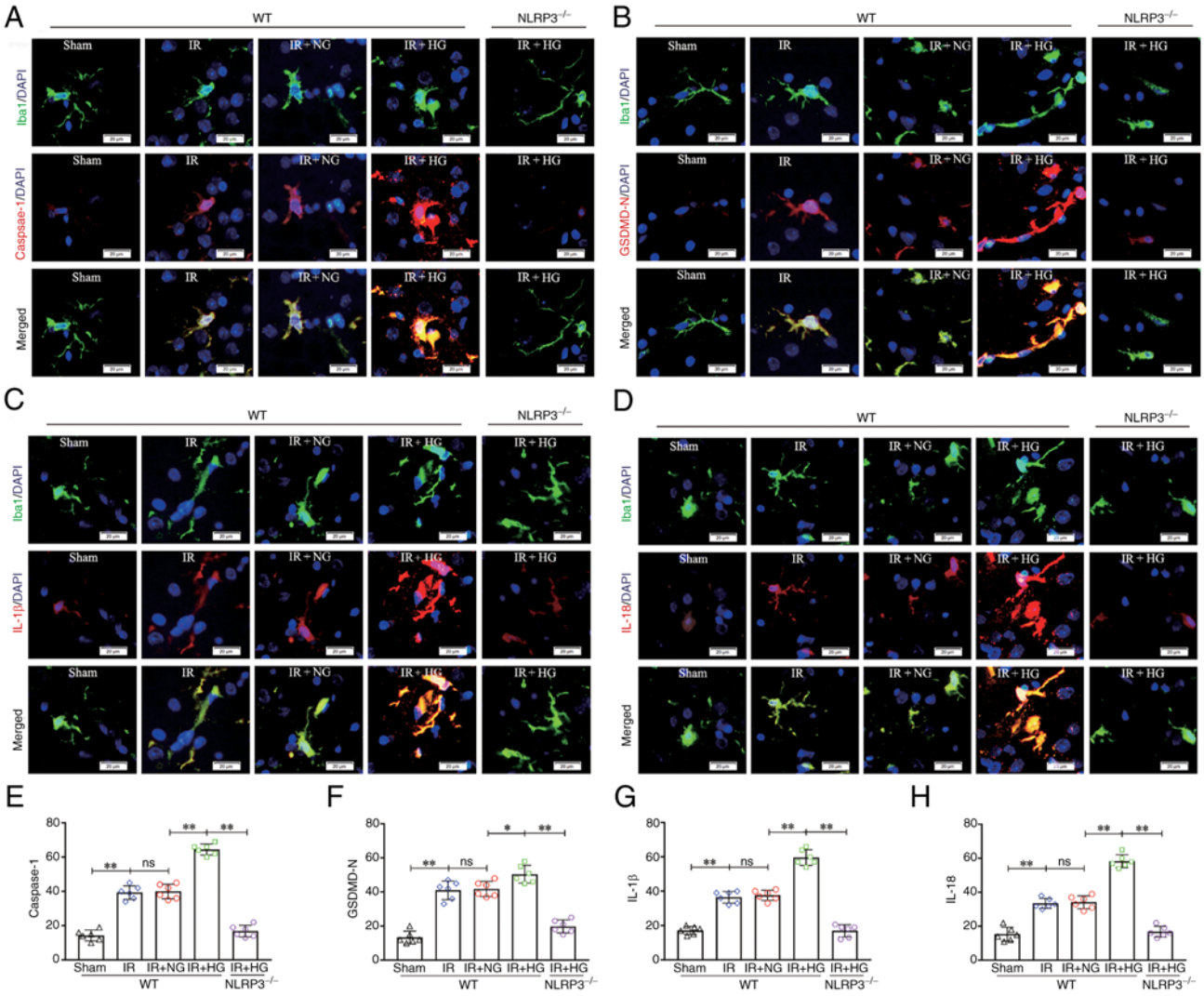

Figure 5. NLRP3$^{-/-}$ inhibited HG-induced exacerbation of microglial pyroptosis after IR *in vivo*. (A) Immunofluorescence images showing the expression of Iba1^{+} microglial cells (green), Caspase-1 (red), and the co-localization of Caspase-1 and microglial cells. (B) Immunofluorescence images showing the expression of Iba1+ microglial cells (green), GSDMD-N (red), and the co-localization of GSDMD-N and microglial cells. (C) Immunofluorescence images showing the expression of Iba1+ microglial cells (green), IL-1β (red), and the co-localization of IL-1β and microglial cells. (D) Immunofluorescence images showing the expression of Iba1+ microglial cells (green), IL-18 (red), and the co-localization of IL-18 and microglial cells. Scale bars (a-i): 20 μm. (E) The fluorescence density of Caspase-1. (F) The fluorescence density of GSDMD-N. (G) The fluorescence density of IL-1β. (H) The fluorescence density of IL-18. Data are presented as the mean ± standard deviation. *P<0.05; **P<0.01; ns, not significant. n=6 mice per group. IR, ischemia-reperfusion; NG, normal glucose; HG, high glucose; NLRP3, NOD-like receptor protein 3; GSDMD-N, gasdermin D-N domain; NLRP3$^{-/-}$; NLRP3 knockout; WT, wild-type.

KO (P<0.01; Fig. 5A and E). IR also enhanced the expression of GSDMD-N in cerebral microglial cells compared with in the Sham group, and this increase was substantially enhanced in the IR group treated with high glucose; however, the expression of GSDMD-N was notably reduced after NLRP3 KO (P<0.01; Fig. 5B and F). IR enhanced the expression of IL-1β in cerebral microglial cells compared with in the Sham group, and this increase was substantially enhanced in the IR group treated with high glucose; however, the expression of IL-1β was notably reduced after NLRP3 KO (P<0.01; Fig. 5C and G). In addition, IR enhanced the expression of IL-18 in cerebral microglial cells compared with in the Sham group, and this increase was substantially enhanced in the IR group treated with high glucose; however, the expression of IL-18 was notably reduced after NLRP3 KO (P<0.01; Fig. 5D and H). These results suggested that NLRP3 KO inhibited high glucose-induced exacerbation of pyroptosis after IR.

NLRP3 KO or inhibition of caspase-1 reverses high glucose-induced exacerbation of pyroptosis after OGD/IR. To evaluate the effect of Z-YVAD-FMK (a caspase-1 inhibitor) on high glucose-induced pyroptosis *in vivo*, the expression levels of caspase-1 were analyzed. The results of western blotting revealed that the expression of caspase-1 was markedly reduced after treatment with Z-YVAD-FMK (P<0.01; Fig. 6A and B). To verify the effect of NLRP3 KO and inhibition of caspase-1 on pyroptosis after OGD *in vitro*, the expression levels of caspase-1, GSDMD-FL, GSDMD-N, IL-1β and IL-18 were analyzed after treatment with high glucose. The results of western blotting revealed an increase in the expression of caspase-1 in the OGD and OGD + NG groups compared with in the CON group (P<0.01), which was further increased in response to high glucose (P<0.01), and a decrease in the expression of caspase-1 was detected in the OGD + HG + NLRP3$^{-/-}$ group and the OGD + HG +

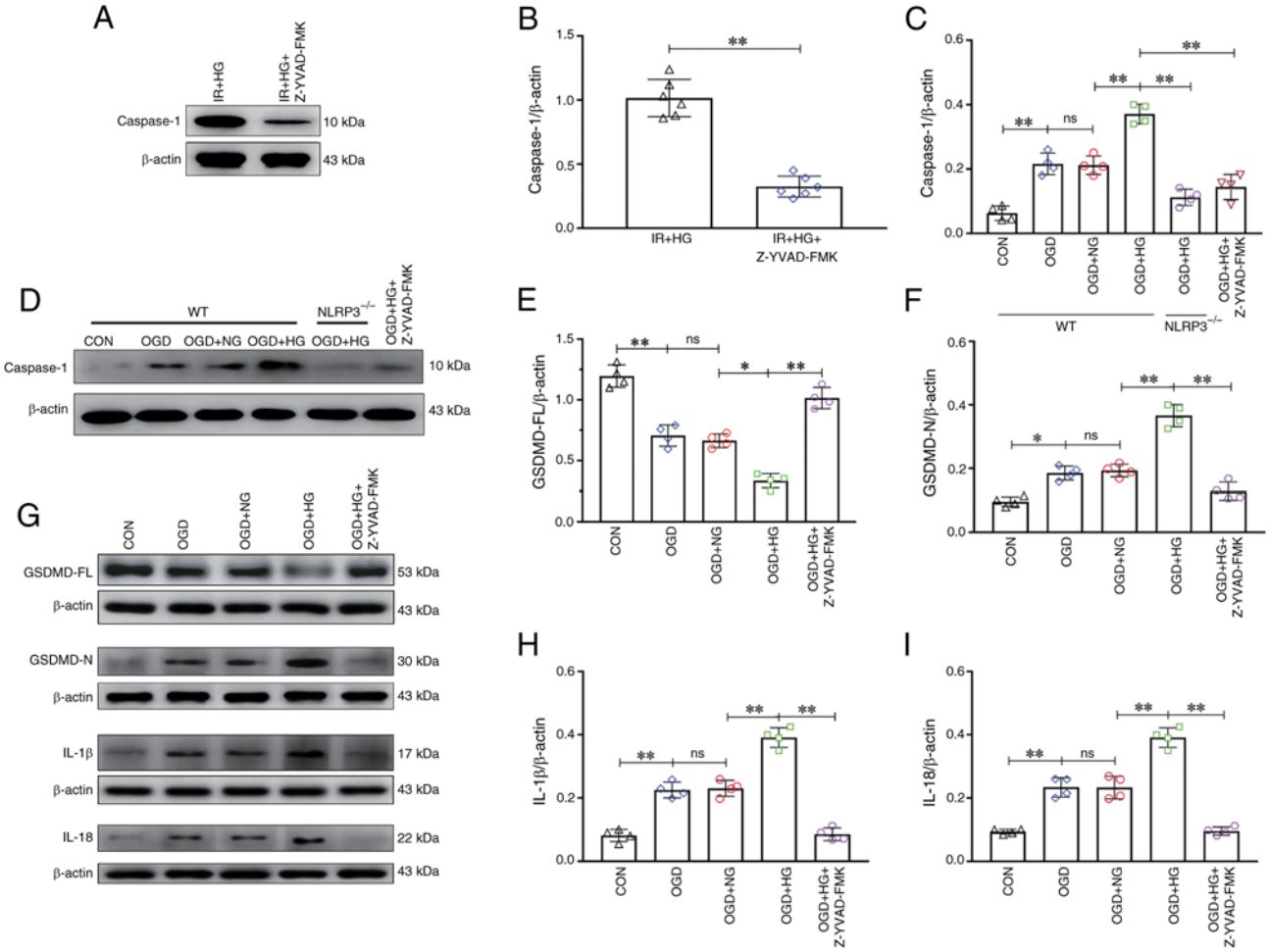

Figure 6. NLRP3$^{-/-}$ and inhibition of Caspase-1 reversed HG-induced exacerbation of pyroptosis after OGD/IR. (A) Western blot analysis of Caspase-1 (10 kDa) *in vivo*. (B) Caspase-1 expression levels *in vivo*. (C) Caspase-1 expression levels *in vitro*. (D) Western blot analysis of Caspase-1 (10 kDa) *in vitro*. (E) GSDMD-FL expression. (F) GSDMD-N expression. (G) Western blot analysis of GSDMD-FL (53 kDa), GSDMD-N (30 kDa), IL-1β (17 kDa) and IL-18 (22 kDa). (H) IL-1β expression. (I) IL-18 expression. Data are presented as the mean ± standard deviation. *P<0.05; **P<0.01; ns, not significant. n=4 per group *in vitro*, n=6 per group *in vivo*. IR, ischemia-reperfusion; OGD, oxygen and glucose deprivation; NG, normal glucose; HG, high glucose; NLRP3, NOD-like receptor protein 3; GSDMD-FL, full-length gasdermin D; GSDMD-N, gasdermin D-N domain; NLRP3$^{-/-}$; NLRP3 knockout; WT, wild-type; CON, control.

Z-YVAD-FMK group compared with in the OGD + HG group (P<0.01; Fig. 6C and D). The expression of GSDMD-FL in the OGD and OGD + NG groups was notably decreased compared with in the CON group (P<0.01), which was further decreased in response to high glucose (P<0.05), and an increase in the expression of GSDMD-FL was detected in the OGD + HG + Z-YVAD-FMK group compared with the OGD + HG group (P<0.01; Fig. 6E and G). The results also revealed an increase in the expression of GSDMD-N in the OGD and OGD + NG groups compared with in the CON group (P<0.05); it was further increased in response to high glucose (P<0.01), and a decrease in the expression of GSDMD-N was observed in the OGD + HG + Z-YVAD-FMK group compared with in the OGD + HG group (P<0.01; Fig. 6F and G). The results revealed an increase in the expression of IL-1β in the OGD and OGD + NG groups compared with in the CON group (P<0.01), which was further increased in response to high glucose (P<0.01), and a decrease in the expression of IL-1β was detected in the OGD + HG + Z-YVAD-FMK group compared with in the OGD + HG group (P<0.01; Fig. 6G and H). Furthermore, the results revealed an increase in the expression of IL-18 in the OGD and OGD + NG groups compared with in the CON group (P<0.01), which was further increased in response to high glucose (P<0.01), and a decrease in the expression of IL-18 was detected in the OGD + HG + Z-YVAD-FMK group compared with in the OGD + HG group (P<0.01; Fig. 6G and I). These results suggested that NLRP3 KO or inhibition of caspase-1 reversed high glucose-induced exacerbation of pyroptosis after OGD/IR.

NLRP3 KO or inhibition of caspase-1 reverses high glucose-induced microglial pyroptosis after OGD. To evaluate the effect of NLRP3 KO and inhibition of caspase-1 on high glucose-induced microglial pyroptosis after OGD *in vitro*, double immunofluorescence was used to examine caspase-1 expression in microglial cells. Enhanced caspase-1 immunofluorescence was observed in the OGD group compared with that in the CON group, and this increase was notably enhanced in the OGD group treated with high glucose; however, the expression of caspase-1 was substantially reduced in the OGD + HG + Z-YVAD-FMK group and the OGD + HG + NLRP3$^{-/-}$ group (P<0.01; Fig. 7A and E). To verify the effect of inhibition of caspase-1

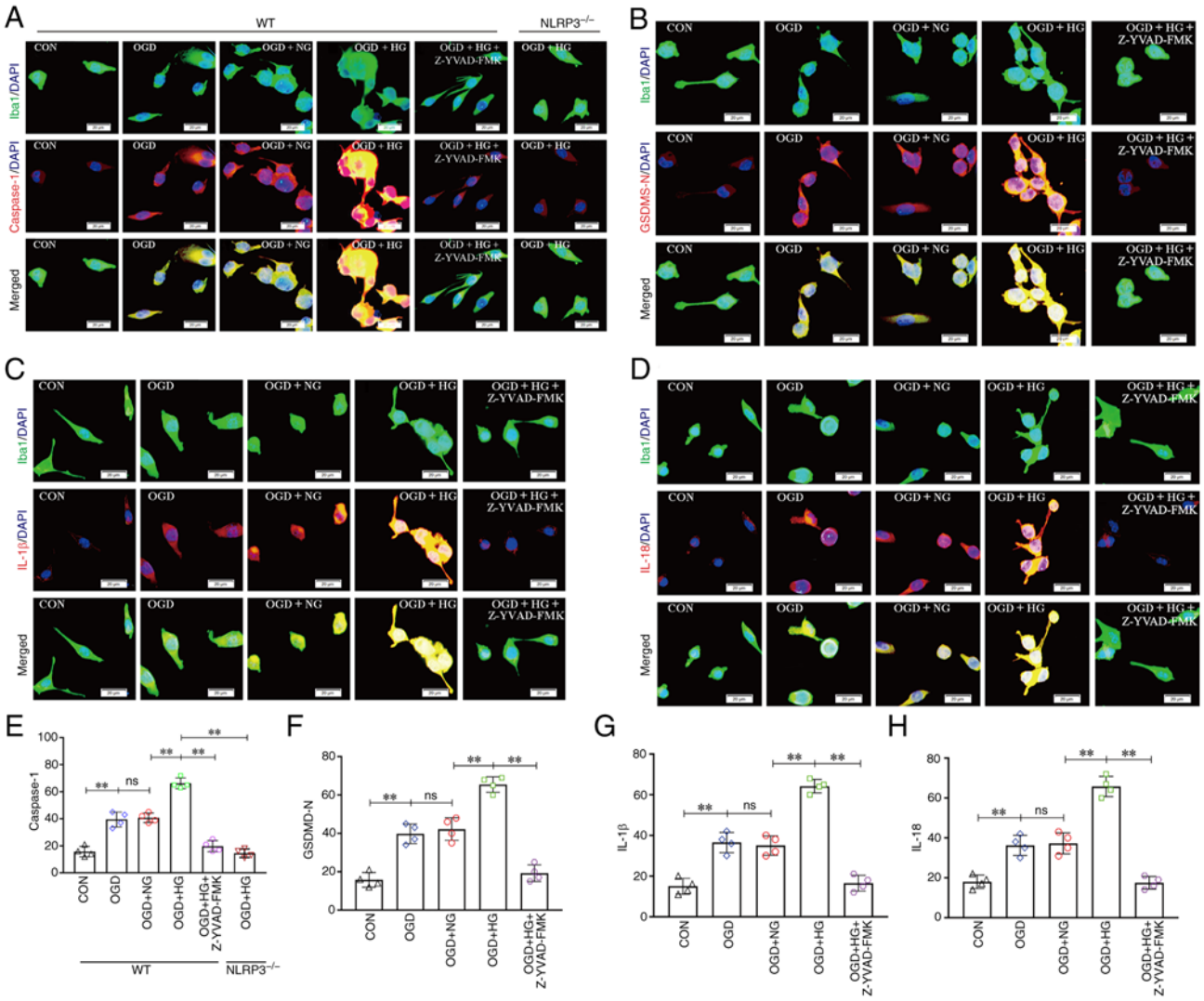

Figure 7. NLRP3$^{-/-}$ and inhibition of Caspase-1 reversed HG-induced exacerbation of pyroptosis after OGD/IR. (A) Immunofluorescence images showing the expression of Iba1^{+} microglial cells (green), Caspase-1 (red), and the co-localization of caspase-1 and microglial cells. (B) Immunofluorescence images showing the expression of Iba1^{+} microglial cells (green), GSDMD-N (red), and the co-localization of GSDMD-N and microglial cells. (C) Immunofluorescence images showing the expression of Iba1+ microglial cells (green), IL-1β (red), and the co-localization of IL-1β and microglial cells. (D) Immunofluorescence images showing the expression of Iba1+ microglial cells (green), IL-18 (red), and the co-localization of IL-18 and microglial cells. Scale bars (a-i): 20 μm. (E) The fluorescence density of Caspase-1. (F) The fluorescence density of GSDMD-N. (G) The fluorescence density of IL-1β. (H) The fluorescence density of IL-18. Data are presented as the mean ± standard deviation. **P<0.01; ns, not significant. n=4 per group. OGD, oxygen and glucose deprivation; NG, normal glucose; HG, high glucose; NLRP3, NOD-like receptor protein 3; GSDMD-N, gasdermin D-N domain; NLRP3$^{-/-}$; NLRP3 knockout; WT, wild-type; CON, control.

on microglial pyroptosis after OGD *in vitro*, double immunofluorescence was used to examine GSDMD-N, IL-1β and IL-18 expression in microglial cells. Enhanced GSDMD-N immunofluorescence was observed in the OGD group compared with that in the CON group, and this increase was notably enhanced in the OGD group treated with high glucose; however, the expression of GSDMD-N was notably reduced in the OGD + HG + Z-YVAD-FMK group (P<0.01; Fig. 7B and F). Enhanced IL-1β immunofluorescence was observed in the OGD group compared with that in the CON group, and this increase was notably enhanced in the OGD group treated with high glucose; however, the expression of IL-1β was notably reduced in the OGD + HG + Z-YVAD-FMK group (P<0.01; Fig. 7C and G). Furthermore, enhanced IL-18 immunofluorescence was observed in the OGD group compared with that in the CON group, and this increase was notably enhanced in the OGD group treated with high glucose; however, the expression of IL-18 was notably reduced in the OGD + HG + Z-YVAD-FMK group (P<0.01; Fig. 7D and H). These results suggested that NLRP3 KO or inhibition of caspase-1 reversed high glucose-induced microglial pyroptosis after OGD.

Discussion

Hyperglycemia is a common complication during ischemic stroke, which is associated with a poorer prognosis with unclear mechanisms (4-7). The present results have shown that hyperglycemia may aggravate hypoxia via increased oxygen extraction rate, as evidenced by the increased $CERO_2$ and OCR, and decreased $PbtO_2$ detected in response to high glucose. The present study, also demonstrated that hyperglycemia

exacerbated neurological impairments during the period of cerebral IR, which was related to more severe pyroptosis in microglia, as evidenced by the increased expression levels of NLRP3, caspase-1, GSDMD-N, IL-1β and IL-18 and a decreased expression level of GSDMD-FL. However, NLRP3 KO suppressed IR-induced pyroptosis aggravation caused by hyperglycemia, and a similar effect was observed in response to a caspase-1 inhibitor.

In patients, ischemic stroke is commonly accompanied by hyperglycemia, which can bring about worse clinical outcomes, including higher morbidity, neurological function destruction, infarct size enlargement and hemorrhagic conversion (18). This has been demonstrated in both non-diabetic and diabetic patients who developed hyperglycemia after stroke and thrombolytic therapy (19). In the present study, the basal blood glucose of mice was within the normal range. Notably, the mice treated with high glucose presented with a more severe neurological impairment after IR, which is consistent with previously reported results (20). Hyperglycemia may lead to worsening of cerebral IR injury via a number of known mechanistic pathways, including damage to the vascular endothelium, increased levels of oxidative stress and overactivation of glial cells (5). However, it remains unclear whether microglial pyroptosis is involved in hyperglycemia-related severe neurological impairment after IR.

In the present study, it was shown that hyperglycemia significantly decreased the levels of $PbtO_2$ in the mice following cerebral IR, and increased the levels of $CERO_2$ and OCR. These results suggested that hyperglycemia aggravated hypoxia by increasing the oxygen extraction rate. This is consistent with the occurrence of pyroptosis in microglia. Pyroptosis is a form of pro-inflammatory programmed necrosis, characterized by caspase-1 activation, rapid plasma membrane rupture, and release of mature IL-1β and IL-18 (21). In the present study, it was revealed that pyroptosis in microglia was triggered after IR, manifested by the upregulated expression levels of NLRP3, caspase-1, GSDMD-N, IL-1β and IL-18 and the downregulated expression level of GSDMD-FL, while it was restrained by NLRP3 KO, which demonstrated that IR induced NLRP3 inflammasome-mediated pyroptosis. There is existing evidence suggesting that hyperglycemia-induced pyroptosis in podocytes, myocardium and macrophages may lead to organ damage in diabetes (22-24). Nevertheless, whether hyperglycemia plays a role in microglial pyroptosis following cerebral IR remains to be elucidated. Furthermore, the present study revealed that high glucose treatment stimulated the aggravation of pyroptosis in microglia after cerebral IR, while this response was significantly suppressed in NLRP3 KO mice and they presented improvements in neurological functions. In addition, the caspase-1 inhibitor Z-YVAD-FMK exhibited a similar inhibitory effect on microglial pyroptosis in microglia treated with OGD and high glucose. These results suggested that hyperglycemia can activate pyroptosis in microglia after cerebral IR through the NLRP3/caspase-1 pathway, and downregulation of NLRP3 and caspase-1 is a potential approach to reduce neural functional injury.

There are two limitations to this study. In the present study, it was exposed that hyperglycemia during ischemic stroke can increase pyroptosis and result in poor neurological outcomes in mice. However, hypoglycemic therapy was not applied to verify whether the timely regulation of blood sugar results in neurological improvement. Additionally, reactive oxygen species (ROS) are known to be critical for pyroptosis (25,26). In the present study, it was shown that hyperglycemia aggravated hypoxia via increasing the oxygen extraction rate. These results suggested that hyperglycemia may induce ROS overproduction be intensifying hypoxia, which could be a possible upstream pathway of pyroptosis, which should be assessed in a future study.

In conclusion, hyperglycemia stimulated NLRP3 inflammasome activation via increasing the oxygen extraction rate, thus leading to the aggravation of pyroptosis following ischemic stroke.

Acknowledgements

Not applicable.

Funding

This work was supported by the National Natural Science Foundation for Young Scientists of China (grant no. 82002074), Natural Science Foundation of Guangdong Province (grant nos. 2023A1515010267 and 2023A1515012665), Ruiyi Emergency Medical Research Fund (grant no. R2021020), Science and Technology Program of Guangzhou (grant no. 202102080003), Medical Scientific Research Foundation of Guangdong Province (grant nos. B2021400, B2022248 and A2021067) and China International Medical Foundation Cerebrovascular Disease Youth Innovation Fund (grant no. Z-2016-20-2201).

Availability of data and materials

The data generated in the present study may be requested from the corresponding author.

Authors' contributions

HZ and HD conceived the study. EL, ZL, SZ, YW and ZY performed the experiments and analyzed the data. All authors read and approved the final version of the manuscript. EL, ZL, SZ, YW, ZY, HZ and HD confirm the authenticity of all the raw data.

Ethics approval and consent to participate

All animal experiments were approved by The Research Ethics Committee of Guangdong Provincial People's Hospital (Guangzhou, China; approval no. GDRECKY2020-046-01).

Patient consent for publication

Not applicable.

Competing interests

The authors declare that they have no competing interests.

References

1. Feske SK: Ischemic stroke. Am J Med 134: 1457-1464, 2021.
2. Tsao CW, Aday AW, Almarzooq ZI, Alonso A, Beaton AZ, Bittencourt MS, Boehme AK, Buxton AE, Carson AP, Commodore-Mensah Y, *et al*: Heart disease and stroke statistics-2022 update: A report from the american heart association. Circulation 145: e153-e639, 2022.
3. Herpich F and Rincon F: Management of acute ischemic stroke. Crit Care Med 48: 1654-1663, 2020.
4. Gray CS, Hildreth AJ, Sandercock PA, O'Connell JE, Johnston DE, Cartlidge NE, Bamford JM, James OF and Alberti KGMM; GIST Trialists Collaboration: Glucose-potassium-insulin infusions in the management of post-stroke hyperglycaemia: The UK glucose insulin in stroke trial (GIST-UK). Lancet Neurol 6: 397-406, 2007.
5. Johnston KC, Bruno A, Pauls Q, Hall CE, Barrett KM, Barsan W, Fansler A, Van de Bruinhorst K, Janis S and Durkalski-Mauldin VLD; Neurological Emergencies Treatment Trials Network and the SHINE Trial Investigators: Intensive vs standard treatment of hyperglycemia and functional outcome in patients with acute ischemic stroke: The SHINE randomized clinical trial. JAMA 322: 326-335, 2019.
6. Desilles JP, Syvannarath V, Ollivier V, Journé C, Delbosc S, Ducroux C, Boisseau W, Louedec L, Di Meglio L, Loyau S, *et al*: Exacerbation of thromboinflammation by hyperglycemia precipitates cerebral infarct growth and hemorrhagic transformation. Stroke 48: 1932-1940, 2017.
7. Ergul A, Li W, Elgebaly MM, Bruno A and Fagan SC: Hyperglycemia, diabetes and stroke: Focus on the cerebrovasculature. Vascul Pharmacol 51: 44-49, 2009.
8. Jia J, Yang L, Chen Y, Zheng L, Chen Y, Xu Y and Zhang M: The role of microglial phagocytosis in ischemic stroke. Front Immunol 12: 790201, 2022.
9. Ding H, Li Y, Wen M, Liu X, Han Y and Zeng H: Elevated intracranial pressure induces IL-1β and IL-18 overproduction via activation of the NLRP3 inflammasome in microglia of ischemic adult rats. Int J Mol Med 47: 183-194, 2021.
10. Song L, Pei L, Yao S, Wu Y and Shang Y: NLRP3 inflammasome in neurological diseases, from functions to therapies. Front Cell Neurosci 11: 63, 2017.
11. Liao LZ, Chen ZC, Wang SS, Liu WB, Zhao CL and Zhuang XD: NLRP3 inflammasome activation contributes to the pathogenesis of cardiocytes aging. Aging (Albany NY) 13: 20534-20551, 2021.
12. Lian H, Fang X, Li Q, Liu S, Wei Q, Hua X, Li W, Liao C and Yuan X: NLRP3 inflammasome-mediated pyroptosis pathway contributes to the pathogenesis of Candida albicans keratitis. Front Med (Lausanne) 9: 845129, 2022.
13. Liu L, Wang N, Kalionis B, Xia S and He Q: HMGB1 plays an important role in pyroptosis induced blood brain barrier breakdown in diabetes-associated cognitive decline. J Neuroimmunol 362: 577763, 2022.
14. Ismael S, Nasoohi S, Yoo A, Ahmed HA and Ishrat T: Tissue plasminogen activator promotes TXNIP-NLRP3 inflammasome activation after hyperglycemic stroke in mice. Mol Neurobiol 57: 2495-2508, 2020.
15. Ardehali MR and Rondouin G: Microsurgical intraluminal middle cerebral artery occlusion model in rodents. Acta Neurol Scand 107: 267-275, 2003.
16. Percie du Sert N, Ahluwalia A, Alam S, Avey MT, Baker M, Browne WJ, Clark A, Cuthill IC, Dirnagl U, Emerson M, *et al*: Reporting animal research: Explanation and elaboration for the ARRIVE guidelines 2.0. PLoS Biol 18: e3000411, 2020.
17. Ding HG, Li Y, Li XS, Liu XQ, Wang KR, Wen MY, Jiang WQ and Zeng HK: Hypercapnia promotes microglial pyroptosis via inhibiting mitophagy in hypoxemic adult rats. CNS Neurosci Ther 26: 1134-1146, 2020.
18. Desilles JP, Meseguer E, Labreuche J, Lapergue B, Sirimarco G, Gonzalez-Valcarcel J, Lavallée P, Cabrejo L, Guidoux C, Klein I, *et al*: Diabetes mellitus, admission glucose, and outcomes after stroke thrombolysis: A registry and systematic review. Stroke 44: 1915-1923, 2013.
19. Li J, Quan K, Wang Y, Zhao X, Li Z, Pan Y, Li H, Liu L and Wang Y: Effect of stress hyperglycemia on neurological deficit and mortality in the acute ischemic stroke people with and without diabetes. Front Neurol 11: 576895, 2020.
20. Li WA, Moore-Langston S, Chakraborty T, Rafols JA, Conti AC and Ding Y: Hyperglycemia in stroke and possible treatments. Neurol Res 35: 479-491, 2013.
21. Yu P, Zhang X, Liu N, Tang L, Peng C and Chen X: Pyroptosis: Mechanisms and diseases. Signal Transduct Target Ther 6: 128, 2021.
22. Qiu Z, Lei S, Zhao B, Wu Y, Su W, Liu M, Meng Q, Zhou B, Leng Y and Xia ZY: NLRP3 inflammasome activation-mediated pyroptosis aggravates myocardial ischemia/reperfusion injury in diabetic rats. Oxid Med Cell Longev 2017: 9743280, 2017.
23. Lin J, Cheng A, Cheng K, Deng Q, Zhang S, Lan Z, Wang W and Chen J: New insights into the mechanisms of pyroptosis and implications for diabetic kidney disease. Int J Mol Sci 21: 7057, 2020.
24. Zhao P, Yue Z, Nie L, Zhao Z, Wang Q, Chen J and Wang Q: Hyperglycaemia-associated macrophage pyroptosis accelerates periodontal inflamm-aging. J Clin Periodontol 48: 1379-1392, 2021.
25. Cui Y, Chen XB, Liu Y, Wang Q, Tang J and Chen MJ: Piperlongumine inhibits esophageal squamous cell carcinoma in vitro and in vivo by triggering NRF2/ROS/TXNIP/NLRP3-dependent pyroptosis. Chem Biol Interact 390: 110875, 2024.
26. Wang J, Yin Y, Zhang Q, Deng X, Miao Z and Xu S: $HgCl_2$ exposure mediates pyroptosis of HD11 cells and promotes M1 polarization and the release of inflammatory factors through ROS/Nrf2/NLRP3. Ecotoxicol Environ Saf 269: 115779, 2024.